

In Silico Based Rank-Order Determination and Experiments on Nonaqueous Electrolytes for Sodium Ion Battery Applications

Ganesh Kamath,[†] Richard W. Cutler,[‡] Sanket A. Deshmukh,^{||} Mehdi Shakourian-Fard,[†] Riley Parrish,[‡] Joshua Huether,[‡] Darryl P. Butt,^{‡,§} H. Xiong,^{*,‡,§} and Subramanian K. R. S. Sankaranarayanan^{*,||}

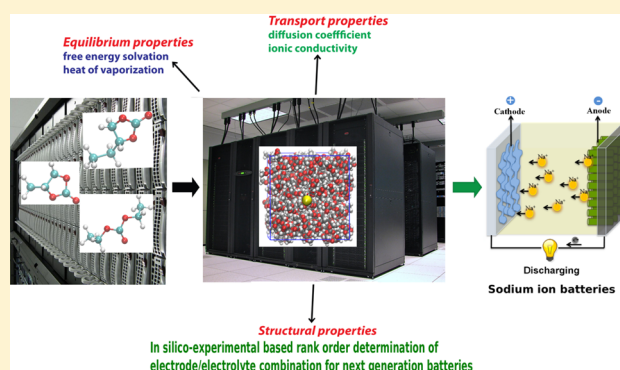
[†]Department of Chemistry, University of Missouri–Columbia, Columbia, Missouri 65211, United States

[‡]Department of Material Science and Engineering, Boise State University, 1910 University Dr., Boise, Idaho 83725, United States

[§]Center for Advanced Energy Studies, 995 University Blvd., Idaho Falls, Idaho 83415, United States

^{||}Center for Nanoscale Materials, Argonne National Laboratory, 9700 S. Cass, Argonne, Illinois 60439, United States

ABSTRACT: Electrolytes are an important component of electrochemical energy storage systems and their optimization is critical for emerging beyond lithium ion technologies. Here, an integrated computational-experimental approach is used to rank-order and aid the selection of suitable electrolytes for a Na-ion battery. We present an in silico strategy based on both thermodynamic and kinetic descriptors derived from molecular dynamics simulations to rationally arrive at optimal electrolytes for Na-ion batteries. We benchmarked various electrolytes (pure and binary mixtures of cyclic and acyclic carbonates with NaClO₄ salt) to identify appropriate formulations with the overarching goal of simultaneously enhancing cell performance while meeting safety norms. Fundamental insights from computationally derived thermodynamic and kinetic data considerations coupled with atomistic-level description of the solvation dynamics is used to rank order the various electrolytes. Thermodynamic considerations based on free energy evaluation indicate EC:PC as a top electrolyte formulation under equilibrium conditions. However, kinetic descriptors which are important factors dictating the rate capability and power performance suggest EC:DMC and EC:EMC to be among the best formulations. Experimental verification of these optimized formulations was carried out by examining the electrochemical performance of various electrolytes in Na/TiO₂ nanotubes half cells with NaClO₄ salt. Our rate capability studies confirm that EC:DMC and EC:EMC to be the best formulations. These optimized formulations have low-rate specific capacities ~120–140 mAh/g whereas the lower ranked electrolytes (EC: DEC) have capacities ~95 mAh/g. The various electrolytes are also evaluated from a safety perspective. Such results suggest encouraging prospects for this approach in the a priori prediction of optimal sodium ion systems with possible screening implications for novel battery formulations.



INTRODUCTION

Rechargeable Lithium-ion battery (LIB) has been the major breakthrough in the field of energy storage technology and is primarily based on insertion of Li ions from the electrolyte into a solid electrode with preferably little change in the electrode host structure and electrolyte properties.^{1–3} The current Li-ion technologies are under intense research and development, but are facing limitations to offer increased energy and power density, improved safety, longer calendar life, and lower cost.^{3–12} There is a tremendous drive toward finding electrical energy storage systems that go beyond Li-ion technologies.^{13–18} Important considerations in alternative battery technologies include low-cost, safe, environmental benign, sustainable rechargeable batteries of adequate energy density, and rate capability.^{8,19–21} Sodium-ion batteries are being touted as a viable alternative candidate^{18,21,22} owing to its enormous abundance and availability, low cost, and its similarity to Li

intercalation chemistries. Despite similar intercalation chemistries, sodium ion batteries are anticipated to have difficulties competing with Li-based batteries in terms of energy density due to their higher equivalent weight and larger ionic size of Na compared to Li. In order to compete and go beyond the existing Li-ion technology, a significant advancement in our understanding of electrodes, electrolytes, and interfacial dynamics is needed.

While substantial recent efforts have focused on electrode materials for sodium-ion batteries,^{23–25} studies involving the identification of optimal electrolytes have remained scarce.^{26–28} Among the various important battery components, the selection of an appropriate electrolyte is a critical consideration

Received: March 10, 2014

Revised: May 19, 2014

Published: May 28, 2014

in the design of next-generation batteries such as Na-ion. Based on available reports,^{26–28} it should be pointed out that the electrolytes and additives, which perform well for Li-ion cells do not guarantee their suitability for Na-ion batteries. For example, vinylene carbonate, which is commonly used as an electrolyte additive in LIBs has been found to be detrimental for Na-ion batteries.²⁸ Hence, a simple extrapolation for the choice of optimal electrolytes for Na-ion from Li-ion chemistry is not possible. The development of next generation electrolytes is catered toward an improved performance and can be based on evaluation of thermodynamic (good solubility) and kinetic properties (high ion mobility/low viscosity), electrochemical, thermal and mechanical stability, (electrochemical window, temperature/pressure parametric), minimization of interface reactions, thereby enhancing cell performances and safety aspects.^{2,26,29} For Na-ion technology to become a practical reality, a systematic investigation of the various solvents and the aforementioned properties is a must.

In this work, we demonstrate that an integrated computational-experimental approach can be used to determine the rank-order based on different objective criteria and aid the selection of suitable electrolytes for a Na-ion battery. While there may be various criteria to narrow down the candidate list from the ever-growing chemical phase space, it is often worthwhile to include both thermodynamic and kinetic considerations for optimization of the best electrode/electrolyte combination. Therefore, we first present an *in silico* strategy based on both thermodynamic and kinetic descriptors to rationally arrive at optimal electrolytes for Na-ion batteries. Fundamental insights from both thermodynamic and kinetic considerations coupled with atomistic understanding of the solvation dynamics is used in rank-ordering the various organic electrolytes (cyclic and acyclic carbonates) and their combinations. We evaluate various electrolytes (pure and binary mixture) and rank-order them based on a) thermodynamic (solubility) b) kinetic factors (ionic conductivity and activation barrier) c) safety (heat of vaporization) factors. In particular, we perform an *in silico* based molecular dynamics simulation (MD) study on a variety of electrolytes and salt combination (NaClO_4). We subsequently verify our rank-order scheme by performing experiments based on titanium dioxide electrodes.³⁰

In designing new electrolytes, it is generally desired that the solubility of the salt in nonaqueous solvents are high. Our basic hypothesis is that for a successful ion-electrolyte system the ion should have a favorable free energy of solvation in a particular electrolyte. As a first rank-order criterion, we perform the potential of mean force (PMF) calculations to extract the free energy of solvation for these different electrolyte-salt combinations in bulk and rank them based on the magnitude of free energy predictions. The energetics of ion solvation is used to understand the surface preference of the intercalating ion for a given electrolyte. With the aid of PMF simulations, we are able to accurately predict the free energies of solvation of these salts in a variety of different nonaqueous liquid electrolytes with the standard deviation from the mean values being in the range of 0.5 to 1 kcal/mol. The PMF calculations provide insights into the solubility of Na salts in the various electrolytes and serve as a metric for choosing the most suitable electrolyte-salt combination for Na-ion batteries.

As a second criterion for rank-ordering electrolytes, we compute the ionic conductivity as well as the activation barriers for Na ion diffusion based on the MD simulation trajectories of Na ions in the various electrolytes. These transport metrics are

used to refine the rank order of the electrolytes, in addition to the thermodynamics and equilibrium considerations. Ionic conductivity is closely linked to key performance metrics of Na-ion battery cells such as rate capability. We also quantify the ionic mobility of the various electrolytes by evaluating the Na ion transport numbers. The atomistic models are also used to explore the intricate relationship between the thermodynamic and kinetic variables to the local coordination/solvation, the short-range ion–solvent interaction and the long-range interionic Coulombic attraction of the Na salt.

As a third criterion, we have also determined the heats of vaporization of the various pure and mixed organic electrolytes. This information will be used to identify the operational range and safety aspects of the electrolytes. Electrolytes with low heat of vaporization can be considered unsafe whereas those with high heats of vaporization can be considered to be safe for operation.

Finally, based on this *a priori* knowledge, we also evaluated the rank-ordering of the electrolytes experimentally by testing the performance of amorphous TiO_2 nanotube³⁰ anode with NaClO_4 salt. TiO_2 is one of the most versatile materials available, and has found its way into many practical applications such as solar cells, catalysts, and pharmaceuticals.³¹ Due to its inertness to chemical environment and relatively low operating electrochemical potential, TiO_2 has long been considered as a good candidate for producing a safe anode.³² Previously, we have demonstrated that amorphous TiO_2 nanotube (TiO_2NT) electrode is a viable anode for Na-ion batteries.³⁰ The well-defined size and morphology of TiO_2 nanotubes make them suitable model system to study the electrode–electrolyte interactions in Na system which can be extended to more complex oxide electrodes. The performances of the TiO_2 nanotube electrode in Na half-cells were found to be commensurate with the computational predictions. Collectively, we demonstrate an integrated *in silico*-experimental approach to rank-order electrolytes based on thermodynamic, kinetic, and thermal properties useful for Na-ion batteries.

METHODS

A.) Computational details. a.) Potential of mean force calculations. We employ the adaptive biasing force (ABF) method developed by Darve and co-workers³³ to calculate the free energy of solvation for the various battery electrolytes. As a part of ABF algorithm, an external biasing force, estimated locally from the sampled conformations of the system and updated continuously, is applied at each step to facilitate the system in overcoming significant energy barriers along the collective variable. This allows the system to evolve freely without constraints, enabling the simulation to visit multiple states separated by high free energy barriers and improving sampling along the reaction coordinate. A unique feature of the ABF method is the use of unconstrained collective variables, thereby enabling unbiased and uniform sampling of the defined region. Using this method we have been able to accurately predict the free energy of solvation, hydration and partition coefficients, of a variety of compounds ranging from alkanes³⁴ to complex fluids such as ionic liquids³⁵ and including exfoliation and stabilization energetics of nanomaterials in ionic liquids.³⁵ Key to the success of any free energy perturbation method using Monte Carlo or MD in predicting macroscopic observables is the intermolecular potential used to describe the pairwise interactions. In this work, an all-atom force field based on the CHARMM General Force field

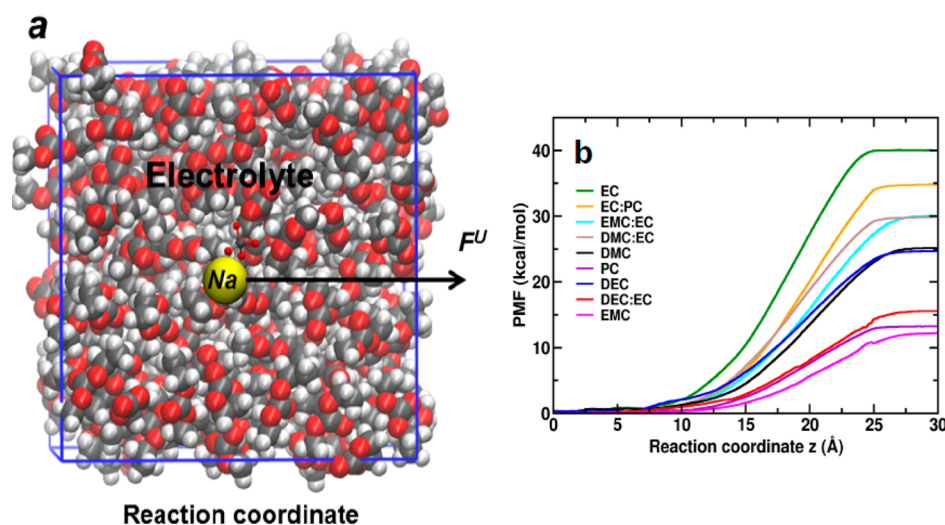


Figure 1. Schematic diagram for the interfacial system consisting of $[\text{Na}]^+$ cation $[\text{ClO}_4]^-$ anion pair placed in the cyclic/acyclic carbonate rich environment, separated from its periodic image in the z direction by vacuum. Six windows whose dimensions were 5 \AA in the z -direction and $\sim 30 \text{ \AA}$ in the x and y -direction each respectively were used to compute the potential of mean force using ABF–MD simulations. The arrow suggests the direction of solute transfer (Na^+ cation) with a force F^U along the z reaction coordinate such that the cation is translocated in a reversible fashion across the Gibbs dividing surface into vacuum. The counterpart of the force is distributed over all the solvent molecules forming the cyclic/acyclic carbonate lamella. Right: Average free energy of solvation profiles generated with ABF–MD for Na^+ cation solvation transferred from a carbonate-rich phase to vacuum. The reaction coordinate is defined in the z -direction.

(CGENFF)³⁶ was used to model the cyclic, acyclic carbonates and the salt interactions.

Here, the ABF method adopted in NAMD³⁷ is used to determine the free energies of solvation for Na^+ cation in different cyclic, acyclic carbonates viz. ethylene carbonate (EC), dimethyl carbonate (DMC), diethyl carbonate (DEC), ethyl methyl carbonate (EMC), propylene carbonate (PC), vinyl carbonate (VC), and butylene carbonate (BC). We have also evaluated four equimolar binary mixtures – EC:PC, EC:EMC, EC:DMC, and EC:DEC. In Figure 1, the left panel shows sodium ion in complex with ClO_4^- anion solvated in a nonaqueous electrolyte. The sodium cation is subjected to a force F and moved from the electrolyte rich phase to vacuum. The free energy of solvation which is based on the integration of the applied force F^U along the reaction coordinate (z) and is computed based on the difference of free energy in electrolyte rich phase and vacuum. The right panel shows the computed free energy profiles of Na^+ cation complexed with ClO_4^- anion in a variety of different cyclic, acyclic carbonates and binary mixtures of cyclic/acyclic carbonates.

b.) Simulation setup. A simulation box was used, whose dimensions were $30 \text{ \AA} \times 30 \text{ \AA} \times 60 \text{ \AA}$, with the cyclic/acyclic carbonate and/or its binary components occupying a region approximately $30 \times 30 \times 30 \text{ \AA}^3$. This cell was extended to 150 \AA in the z -direction with a 90 \AA vacuum region. The vacuum region was necessary to prevent interactions of the solute in the condensed phase with its image through periodic boundary conditions. The number of molecules in each box was selected to reproduce the density of cyclic/acyclic carbonate predicted by NPT simulations at 1 atm and 300 K for a specific potential truncation (14 \AA). The initial distribution of salt ion (solute) is random and therefore homogeneous through the various different bulk electrolytes. The free energy is computed based on the force F^U exerted on the solitary Na^+ ion. The collective variable for the determination of free energy changes was defined as the distance between the center of mass of the solute (COMS) under study and center of mass of the condensed

phase (COMCP). In the initial system setup, the COMS was placed at approximately the COMCP. Over the course of simulation, the reaction coordinate spanned a distance of 30.0 \AA from COMCP to the center of the vacuum region. To reduce the statistical error of the calculations, the reaction pathway was divided into six equally sized non-overlapping windows of 5.0 \AA . To generate the initial configurations for each window, a single 30 ns ABF run was performed spanning the complete pathway from 0.0 \AA to 30.0 \AA after heating and equilibration of the system. Coordinates from the trajectory of this simulation were saved periodically to generate five initial coordinate files for the five windows. Force statistics were stored in bins of width 0.02 \AA . The biasing force was applied after every 500 samples were collected in each bin. To keep the solute within the specified window, a harmonic force with a magnitude of $10.0 \text{ kcal mol}^{-1} \text{ \AA}^{-1}$ was applied on the upper and lower boundary of the window along the z axis of the simulation box. A final production run of 30 ns for each window was performed.

c.) MD Simulation details. Molecular dynamics simulations were performed with NAMD.³⁸ The initial configurations for each system were generated with Packmol software. Energy minimization on the system was performed for 500 steps using the steepest decent algorithm. Subsequently the systems were equilibrated over a simulation time period of 20 ns in the isobaric–isothermal (NPT) ensemble at 1.0 atm and 300 K, followed by the ABF–MD calculation using the isothermal NVT ensemble. For all calculations, the temperature was maintained at 300 K using Langevin dynamics. For the NPT simulations, constant pressure was maintained at 1.0 atm using the Nosé–Hoover algorithm. A 1.0 fs time step was used for the integration of Newton’s equation of motion. Periodic boundary conditions were used in all the three spatial coordinates. Long-range electrostatic interactions were calculated with Particle–mesh Ewald algorithm. A switching function was applied for all Lennard–Jones interactions at 12.5 \AA for 14.0 \AA cut–off.

d). *Calculation of ionic conductivity and diffusion barrier.* The ionic conductivity (σ) for Na ion in the various nonaqueous electrolytes can be estimated based on the diffusion coefficients using the Nernst–Einstein equation:³⁹

$$\sigma = \frac{Nq^2D_i}{fk_B T} \quad (1)$$

Here, N is the density of the charge carriers per unit volume and q is the charge on the charge carrier. Here, the charge carrier is the Na⁺ ion, f is the Haven ratio, T is the system temperature, and k_B is the Boltzmann constant. The Haven ratio in this case has been taken as 1. The Na-ion diffusion coefficients are computed from the slope of the mean square displacements evaluated over the 300 K–400 K range ($T = 300$ K, 325 K, 350 K, 375 and 400 K). The diffusion coefficient, D_i , can be derived from the time observed mean square displacement of the molecules using the following equation:

$$\langle r_i^2(t) \rangle = 6D_i t + C \quad (2)$$

where C is the Debye–Waller factor. The activation energy barriers associated with the ionic diffusion in the 300 K–400 K range are then calculated using the standard Arrhenius equation:

$$D_i = A \exp\left(\frac{E_B}{k_B T}\right) \quad (3)$$

e.) *Calculation of heat of vaporization.* The heat of vaporization calculations were performed as follows: Pure solvent MD simulations consisted of 250 molecules in a periodic cubic box. To obtain converged results three independent MD simulations were run for 5 ns with different initial velocities assigned to the particles. The first 1 ns of the simulations were treated as equilibration and the final 4 ns were used in the analysis, and averages were obtained from the three independent simulations. The heat of vaporization ΔH_{vap} was determined using the following expression

$$\Delta H_{\text{vap}} = \langle U \rangle_{\text{molecule}} - \frac{\langle U \rangle_{\text{box}}}{N} + RT \quad (4)$$

where $\langle U \rangle_{\text{box}}$ is the average potential energy of the condensed phase simulation, N is the number of molecules in the periodic box, $\langle U \rangle_{\text{molecule}}$ is the average potential energy of the molecule in the gas phase using infinite nonbonded cutoffs, R is the universal gas constant, and T is the temperature of the condensed phase and gas phase simulations. In the case of mixed solvents, $\langle U \rangle_{\text{molecule}}$ is the average potential energy of the more volatile molecule in the gas phase.

B.) Experiments. i). *Electrolyte preparation.* All tested electrolytes consist of a 1 M NaClO₄ in pure or binary solvent mixtures (1:1 by volume) from propylene carbonate (PC, Aldrich, anhydrous, 99.7%), ethylene carbonate (EC, Aldrich, anhydrous, 99.0%), dimethyl carbonate (DMC, Aldrich, anhydrous, >99%), diethyl carbonate (DEC, Aldrich, anhydrous, 99.0%), and ethyl methyl carbonate (EMC, Aldrich, 99.0%). Solvents were used as received. All chemicals were handled in an Ar-filled glovebox to avoid air and moisture exposure.

ii). *Synthesis of TiO₂ nanotube electrodes.* TiO₂ nanotubes were synthesized by electrochemical anodization method described previously.^{30,40,41} Pure titanium foil (99.8%, Alfa Aesar) was ultrasonically cleaned by acetone, isopropyl alcohol,

and deionized water before anodization. The back of the Ti foil was protected by adhesive to ensure uniform current distribution. The anodization was carried out in a two-electrode cell with Ti metal as the working electrode and a Pt mesh as the counter electrode under a potential of 25 V at room temperature using electrolytes of formamide with 0.8 wt % ammonium fluoride (Aldrich) and 5 vol % D.I. water. The as-anodized samples were ultrasonically cleaned in D.I. water for 30 s. All amorphous TiO₂NT samples were vacuum annealed at 110 °C overnight before assembly in electrochemical cells.

iii). *Electrochemical Characterization.* Na half-cells were assembled in coin-type cells (Hohsen 2032) with TiO₂ nanotube as the positive electrode, a Na metal foil (Aldrich, 99.9%) as the negative electrode and glass fiber separator (Whatman GF/F). TiO₂ nanotube film was grown directly on Ti current collector without adding any carbon additives and polymer binders. Half-cells were cycled galvanostatically at varying currents between 2.2 and 0.6 V or 2.5 and 0.5 V vs Na/Na⁺ using an automated Maccor battery tester at ambient temperature. Electrodes removed from cells for analysis were thoroughly washed with dry DMC (Aldrich) and allowed to dry under inert atmosphere. All cell assembly and disassembly operations were performed in an Ar-filled dry glovebox (oxygen level <0.5 ppm). The actual mass of the TiO₂ nanotube films were determined by peeling off the nanotube film from Ti substrate using adhesives and measuring the weight difference. The remaining substrate was examined by SEM to make sure that no residual TiO₂ nanotube was left on the substrate.

RESULTS AND DISCUSSION

(a). *Free energy of solvation from PMF calculations for Na ion battery electrolytes.* With the aid of PMF simulations, we are able to accurately predict the free energies of solvation of the sodium salts in a variety of electrolytes. The free energy of solvation for different electrolyte-salt combinations in bulk (EC, EMC, DEC, DMC, PC, BC, VC, PC:EC, EMC:EC, DMC:EC, and DEC:EC) is computed and used to rank them based on the free energy predictions. The profiles of the PMF for Na⁺ cation in the different carbonate systems as a function of distance along the reaction coordinate are presented in Figure 1(b). The Gibbs free energy of solvation is defined as the Gibbs free energy change associated with transferring a solute from vacuum to the condensed phase. The free energy of solvation was computed based on the difference in the free energy of the first window (solute in carbonate-rich phase) and the last window (solute in vacuum phase).

The energetics of ion solvation is used to understand the solubility and solvation characteristics of the Na ion for a given electrolyte. The differences in the free energies of sodium cation in the seven pure carbonate solvents and four binary mixtures of carbonates are presented in Figure 2. The higher the magnitude of absolute free energy of solvation of ion in a particular electrolyte under consideration, the more is the affinity for the particular ion in that electrolyte. The rank order for the sodium ion in the carbonates and their binary mixtures based on the free energies of solvation ranging from maximum to minimum affinity toward each electrolyte was found to be EC > EC:PC > EMC:EC ~ DMC:EC > DMC ~ DEC > BC > DEC:EC > VC > PC > EMC.

To provide an atomistic picture behind the differences in the free energy of solvation, we analyze the atomistic interactions that govern the nature of the solvation shell of Na⁺ ions and the resulting ion complexes in the various nonaqueous electrolytes.

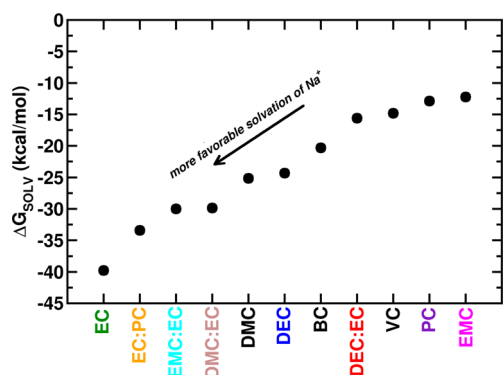


Figure 2. Comparison of the free energy of solvation of sodium cation in various acyclic/cyclic carbonates and their binary mixtures as predicted using ABF–MD simulations at 300 K. The standard deviation of the free energy estimates are within 1 kcal/mol.

The solvation behavior of the Na^+ cation in the various electrolytes is dictated by its coordination with the surrounding oxygen of the carbonates in the first solvation shell. Based on our MD simulation trajectories, we find that the Na^+ ion interacts strongly with the carbonyl ($\text{C}=\text{O}$) oxygen of the carbonates. As seen in the carbon–oxygen RDF shown in Figure 3a, the peak intensities and the nearest neighbor distances suggest that Na^+ ion interacts weakly with the ether oxygen in the alkyl carbonates. This is primarily due to the steric hindrance from the backbone carbons of the carbonates shielding the interaction of the Na^+ ion with the oxygen. However, the carbonyl oxygen projects out of the carbonate molecular surface and hence is easily accessible to interact with the sodium ion. The radial distribution functions computed from our MD trajectories reveals that the $\text{Na}^+ \text{-O}^{2-}$ interaction distance is $\sim 2.5 \text{ \AA}$ which defines the width of the first solvation shell. Figure 3b shows the number integral calculated for 10 ns of Na^+ in solvent under NVT conditions at $T = 300 \text{ K}$. The value corresponding to a cutoff distance of 2.5 \AA gives the oxygen coordination for the first solvation shell.

It is observed that oxygen coordination around a Na^+ ion in the case of pure solvents is $\sim 3\text{--}3.5$ for EMC, PC, and BC whereas DMC and DEC are $\sim 4\text{--}4.5$ and EC is the highest with ~ 5 . Among the binary mixtures, Na^+ ion in DEC:EC has an oxygen coordination ~ 3 whereas Na^+ ion in DMC:EC has a high oxygen coordination ~ 5 and the highest is $\sim 5.5\text{--}6$ for

PC:EC and EMC:EC. For comparison, Li^+ ion usually allows no more than 4 solvent molecules in its solvation shell due to its small ionic radius.² The rank order for pure solvents based on the free energies of solvation ranging from maximum to minimum affinity is $\text{EC} > \text{DMC} \sim \text{DEC} > \text{BC} > \text{VC} > \text{PC} > \text{EMC}$ whereas for binary mixtures, it is found to be $\text{PC:EC} > \text{EMC:EC} \sim \text{DMC:EC} > \text{DEC:EC}$. Thus, the extent of oxygen coordination of Na^+ ions is directly correlated to the free energy of solvation of the electrolyte as well as the stability of the resulting ion–solvent complex.

The best description for the observed variation in the solvation free energies may be that the solvation shells of the Na^+ and ClO_4^- ions are complete only when oxygen coordination is $\sim 5\text{--}6$, and remain incomplete for low coordination ~ 3 . The low oxygen coordination is seen to increase the solvation free energy, thereby increasing the driving force required for equilibration of the ion concentration gradients (see Results and Discussion on transport number in the next section). The solvation shell for high oxygen coordination can be estimated to shield the interionic Coulombic attraction to form close ion pairs that leads to a reduction in the ionic mobility.

At the atomistic level, there is a very intricate relationship between the local coordination/solvation, the short-range ion–solvent interaction, and the long-range cation–anion interaction of the Na salt. The atomistic interactions in the nonaqueous electrolytes can be divided into long-range ion–ion Coulombic interactions and short-range ion–solvent interactions.⁴² Both the short-range ion–solvent and the long-range ion–ion interactions directly relate to the degree of dissociation of the salt, which depends on the dielectric constant of the solvents.

In the case of solvents with low dielectric constant such as EMC, BC, DMC, and even DEC (Table 1), we observe that the oxygen coordination of Na^+ is < 3 in the first solvation shell (see Figure 3 and snapshots shown in Figure 4). For such low coordination complexes, the charge on the Na^+ ions cannot be effectively neutralized through solvation and instead the charge is neutralized by formation of neutral ion pairs.² The electrostatic forces between the ions become therefore more predominant in such solvents, which leads to very high stability of these ion-pair complexes. The high ion pair stability is thus a manifestation of the lower degree of dissociation and is expected to eventually translate into poor ionic mobility.

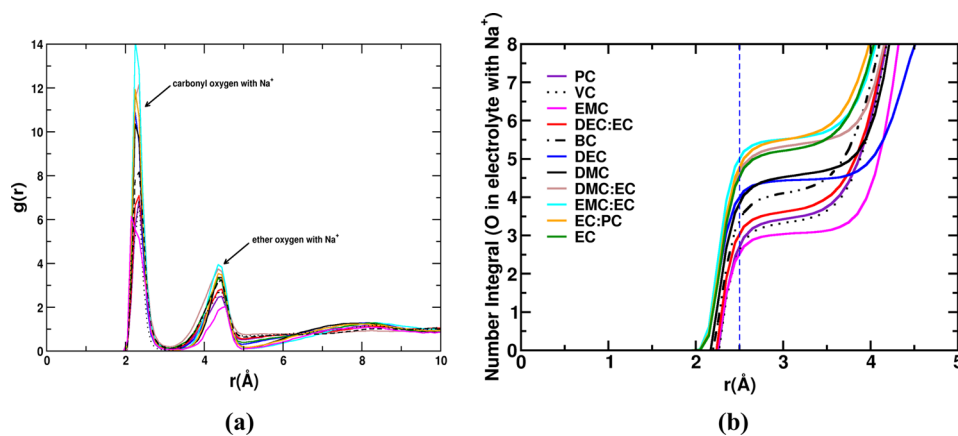


Figure 3. (a) Radial distribution function between carbon and oxygen (b) Number integral calculated from 10 ns of NVT–MD simulations for Na^+ cation with the carbonyl and ether-oxygen of different carbonates and binary mixtures.

Table 1. Dielectric constant,²⁶ viscosity,^{2,26} and transport number of the Na⁺ cation for the various electrolytes. * indicates estimates based on our MD simulations

Electrolyte	Dielectric constant	Viscosity (cP)	Transport Number*
EC	89.78	1.95	0.49
PC	64.92	6.8	0.44
DMC	3.11	0.5	0.44
DEC	2.81	0.3	0.34
VC	--	--	0.30
BC	--	--	0.49
EMC	2.96	0.65	0.44
EC:PC	--	5.3	0.51
EC:DMC	--	2.2	0.49
EC:DEC	--	2.7	0.41
EC:EMC	--	--	0.49

On the other hand, EC has a high dielectric constant of 89.78, which is even higher than the most common solvent of water (~ 79). In the case of EC and its binary mixtures such as EC:PC, EC:EMC, and EC:DMC, we find that the oxygen coordination of Na⁺ ion is ~ 5 – 6 (see Figure 3 and snapshots shown in Figure 4). In such solvents, the charge on the Na⁺ ions is effectively neutralized through solvation and hence the ion–solvent interactions are dominant. Thus, for solvents with high dielectric constant or in other words high oxygen coordination Na⁺ complexes, the stability of the complex is a direct consequence of favorable Na⁺ ion–solvent short-range interactions. The larger number of solvent molecules (especially the interaction of carbonyl oxygen with Na⁺) results in more favorable solvation free energies and maybe in part responsible for better “charge-balance” between the solvent and Na⁺. We observe that the ether oxygen in cyclic and acyclic carbonates interact weakly for distances > 5 Å and thus the interaction of carbonyl oxygen with Na⁺ is governing the short-range interactions.

(b). Experimental evaluation. Experimentally, we examined the electrochemical performance of amorphous TiO₂NT electrode in various electrolytes containing 1 M NaClO₄ in single solvent (PC) and binary solvent mixtures (EC:EMC,

EC:DEC, EC:DMC, and EC:PC) at low current rate ($\sim C/20$) to resemble equilibrium conditions. Figure 5(a) displays the first cycle voltage profiles of TiO₂NT electrode in different electrolytes. The initial voltage profile exhibits a solid solution intercalation mechanism which is consistent with what we have observed previously.³⁰ The initial discharge voltage profile, which is related to processes such as Na⁺ solvation/dissociation, migration, diffusion, desolvation, insertion into host materials, as well as electrolyte decomposition upon reduction, indicates that the degree of voltage loss under the same load between 2.5–1 V (electrolyte decomposition may occur during reduction at voltages below 1 V) from low to high follows the order: EC:EMC < EC:DMC \sim EC:PC < PC \sim EC:DEC. Generally, there are three major contributions to the voltage loss: (a) activation polarization loss, (b) ohmic loss, and (c) concentration loss.⁴³ As the tested cells were operated at a slow rate ($\sim C/20$), the contribution from concentration loss can be considered less significant. Therefore, the voltage loss of TiO₂NT electrode in the initial discharge between 2.5–1 V can be ascribed to the effects from ohmic loss (electrolyte) and activation polarization loss (electrode/electrolyte). We notice that the rank-order observed experimentally matches quite well with theoretical prediction except in the case for EC:PC. We attribute this difference to the possible activation polarization during the charge transfer across the electrode/electrolyte interface when PC is involved in the solvent. As shown in Figure 4, solvation shells at equilibrium mostly consist of solvents with high dielectric constant such as EC and PC. Therefore, solvent molecules in the solvation shells will be possibly more involved in the reductive process at the electrode during discharge than the noncoordinating solvents. The exact mechanisms dictating the charge-transfer process as well as the formation of possible solid electrolyte interface (SEI) layer are not clear and studies on the mechanisms are currently underway in our group.

The initial discharge capacities of the TiO₂NT electrode in various electrolytes are within the range of 200–260 mAh/g (Figure 5a), however, significant irreversibility is observed for all systems tested. The initial Coulombic efficiency is within the

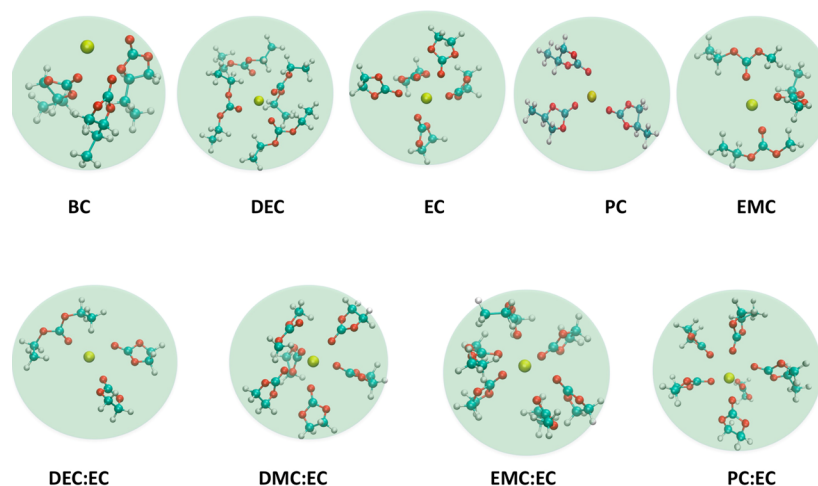


Figure 4. Snapshots from MD simulations showing the local oxygen coordination of Na⁺ cation within the first solvation shell for the various nonaqueous electrolytes. Top panel shows the pure solvents whereas bottom panel shows the snapshots for the mixed solvents. It can be seen that oxygen coordination around a Na⁺ ion is ~ 3 for EMC, PC and BC whereas DMC and DEC are ~ 4 and EC is the highest with ~ 5 . Among the binary mixtures, Na⁺ ion in DEC:EC has an oxygen coordination ~ 3 whereas Na⁺ ion in PC:EC and DMC:EC have a high oxygen coordination ~ 5 and the highest is ~ 6 for EMC:EC.

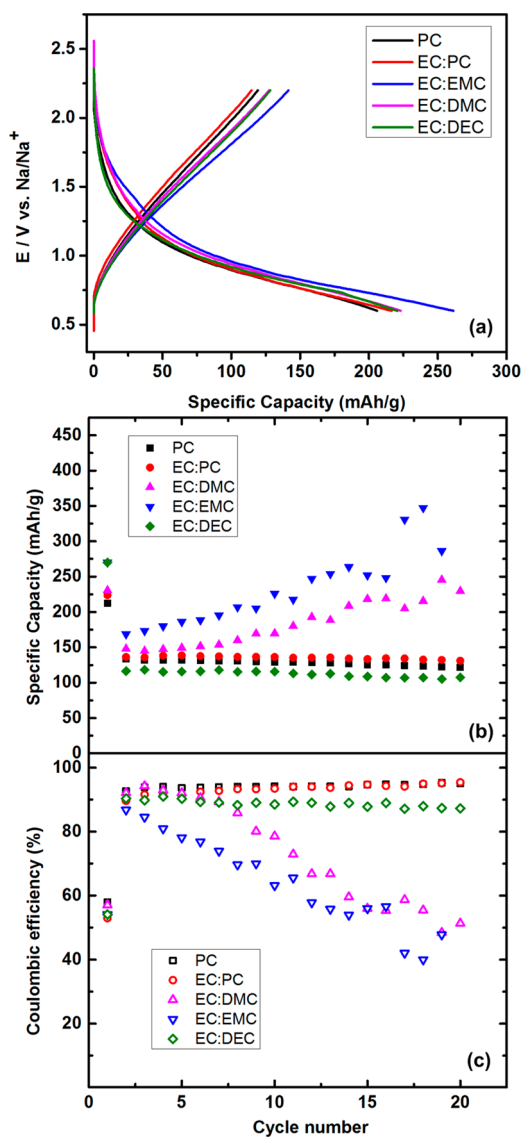


Figure 5. (a) First cycle voltage profiles for amorphous TiO₂/NT electrodes cycled in 1 M NaClO₄ in various solvents at $\sim C/20$ rate. (b) Discharge capacity vs cycle number for the corresponding cells. (c) Coulombic efficiency vs cycle number for the corresponding cells. Error bars are within the symbols.

range of 50–60%. We believe that major contribution of the irreversibility is from side reactions between TiO₂/NT electrode and the electrolytes. Further structural and surface characterizations of the side reaction products are needed to elucidate processes of such reactions. For all the testing cells, the discharge capacities dropped after the initial cycle. Reversible capacities for EC:PC, PC and EC:DEC were observed in successive cycles. For EC:EMC and EC:DMC, it was found that discharge capacities increased with cycles, however, Coulombic efficiency decreases apparently with cycles. The discrepancy is ascribed to possible formation of unstable SEI layers that react to the electrolytes at each discharge. The exact reason is unclear at this stage and further surface analysis is currently carried out in the group to elucidate the interfacial chemistry. The capacity of TiO₂/NT electrode in various electrolytes at low rate follow the order: EC:EMC > EC:DMC > EC:PC \sim PC > EC:DEC. This order agrees with the theoretical predictions.

c). Ionic conductivity for Na diffusion in the electrolytes. Ionic conductivity and diffusion properties of Na salts in the nonaqueous electrolytes determine some of the key performance metrics of Na⁺-ion battery cells like rate capability. Figure 6a shows the calculated ionic conductivity for NaClO₄ in

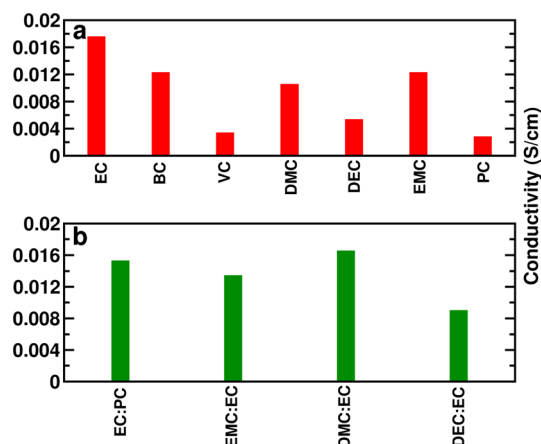


Figure 6. Room temperature ionic conductivity values for systems with 0.1 M of Na salts dissolved in various (a) pure solvents and (b) solvent mixtures.

single carbonate solvents (EC, BC, VC, DMC, DEC, EMC, and PC). It can be seen that the ionic conductivity of pure solvents follows the rank order EC > BC \sim EMC > DMC > DEC > PC > VC. Pure solvents such as EC display an ionic conductivity of ~ 18 mS/cm whereas PC displays an ionic conductivity of ~ 3 mS/cm.

In order to evaluate the role of the cosolvent, we add EC (which performed best on the free energy of solvation as well as the ionic conductivity metric) to form binary equi-molar mixtures of EC:PC, EC:EMC, EC:DMC, EC:DEC. As seen in Figure 6 (b), the addition of EC as a cosolvent resulted in a strong improvement in ionic conductivity in all the cases. The synergetic effects of cosolvent has long been observed in Li system.^{2,44} The highest ionic conductivity is seen for EC:DMC (ca. 18 mS/cm) followed by EC:PC (ca. 16 mS/cm) and EC:EMC (ca. 13 mS/cm). The lowest among the simulated organic mixed solvents is seen for EC:DEC which has an ionic conductivity of ~ 9 mS/cm.

The ionic conductivity of the solvents is dictated by several factors. Some of the most critical ones include (a) the dielectric constant which dictates the degree of dissociation of the salts (b) the viscosity of the solvents which is inversely related to the ionic mobility and (c) the transport number which depends on the relative mobility of the Na⁺ cation to its counteranion. The dielectric constant and the viscosity values for the organic solvents simulated in this work is available in literature^{2,26} and is summarized in Table 1.

Based on the dielectric constants, it can be seen that EC has a value of ~ 89.78 . Therefore, EC and its binary mixtures have high degree of dissociation and as explained earlier have dominant ion–solvent interaction, which screens long-range cation–anion electrostatic attractions. EC also has a low viscosity of 1.95 cP. EC as a pure solvent displays high ionic conductivity and its addition as a cosolvent results in significantly improved ionic conductivity of the mixture. Other solvents such as DMC, DEC, VC, and BC have low dissociation constants and hence have lower ionic conductivity

when compared to EC-based electrolytes. It should be noted that while PC also has a high dielectric constant of 64.9, it also has a high viscosity of 6.8 cP, which explains its poor ionic conductivity.

We further quantify the ionic mobility of the electrolytes by evaluating the Na^+ transport numbers. The transport number is calculated based on the diffusivity of the Na^+ and ClO_4^- ions from the 10 ns MD simulation trajectories. The transport number is defined as the fraction of the net charge carried by the cations out of the total charge passing across a reference plane:⁴

$$t^+ = \frac{D_+}{D_+ + D_-} \quad (5)$$

In the above equation, D_{\pm} are the mobility and the diffusion coefficients of the cations and the anions, respectively.

Table 1 summarizes the Na^+ transport numbers for the various solvents. It can be seen that EC has a high transport number $t^+ = 0.49$, which suggests that fraction of charge transport by the cations and anions, is similar. The EC-based binary solvents also have high Na^+ transport numbers ~ 0.5 for EC:PC \sim EC:DMC \sim EC:EMC with EC:DEC showing a somewhat lower transport number of ~ 0.41 . The observed variation in the transport number is consistent with the ionic conductivity variation shown in Figure 6. Note that the transport numbers for Li^+ in liquid electrolytes commonly used in Li ion batteries (EC and PC) have been reported to be typically less than 0.4.² For example, the Li transport numbers in electrolytes such as EC are in the range of ~ 0.4 whereas they are ~ 0.5 for Na. A transport number of ~ 0.4 for Li suggests that the anions are more mobile than the cations. The small cation current portion is believed to be caused by the high surface charge density on the cations due to their small ionic radii.² In the case of Na, however, there is an equal contribution from both cations and anions and hence the transport numbers are ~ 0.5 . Hence the transport numbers for EC-based electrolytes in general suggests their suitability for Na-ion batteries. We observe that DMC and EMC have a somewhat lower transport number ~ 0.44 whereas BC surprisingly displays a higher $t^+ = 0.49$. The low transport numbers $t^+ = 0.30$ and 0.34 obtained in the case of VC and DEC, respectively shows that Na^+ carries only a small fraction of the charge. Since the charge is also carried by the counterions, a concentration gradient develops in the case of solvents with low transport numbers, which does not augment well for battery operation.

d). Activation barrier for Na^+ ion diffusion. We evaluate the activation barrier for Na^+ ion conduction in the various electrolytes in the temperature range 300 K–400 K. Considering that the ionic conduction can be the rate-determining process compared to electronic conduction in an electrochemical reaction, it is important to consider kinetic factors such as the activation barrier for Na ion diffusion. In liquid electrolytes, diffusion is governed by random jumps of atoms or ions, leading to position exchange with their neighbors. The kinetics of this process is temperature dependent and follows an Arrhenius-type relationship, which was used to extract the Na^+ diffusion barrier in the 300–400 K range. The same is shown in Figure 7 for the various neat and mixed electrolytes.

It can be seen that among the pure solvents, PC presents the highest activation barrier. This is not surprising since the viscosity of PC is ~ 6.8 cP which is considerably higher than

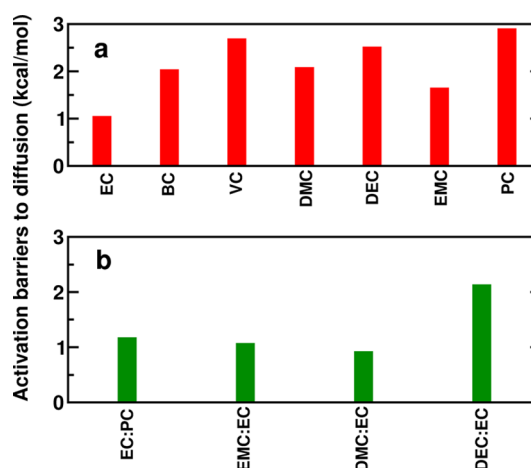


Figure 7. Activation barrier for ionic diffusion calculated for systems with 0.1 M of Na salts dissolved in various (a) pure solvents and (b) solvent mixtures.

other pure solvents (Table 1). EC presents the lowest barrier among the simulated pure solvents. The rank order of ionic mobility based on decreasing Na^+ diffusion barrier is EC > EMC > BC \sim DMC > DEC > VC > PC. At the macroscopic level, it appears that the viscosity of the solvent primarily dictates the diffusion barrier.

At the atomistic level, the solvation shell around a Na^+ ion is incomplete in the case of pure solvents such as PC, VC, EMC, and BC (oxygen coordination is ~ 3 – 3.5) whereas for DMC and DEC, they are more complete (oxygen coordination are ~ 4 – 4.5) and EC has the most complete solvation shell with ~ 5 . In the case of solvents with incomplete solvation shells, the electrostatic interactions between the salt ions are not effectively screened. As a result, the interionic attractions dominate over the ion–solvent interactions. The long-range electrostatic attractions lead to the formation of high stability ion-pair complexes, which reduce ion mobility and lead to an increased activation barrier for diffusion. The addition of EC as a cosolvent to PC, EMC, and DMC leads to an increase in oxygen coordination and the ion–solvent interactions become dominant leading to a reduction in the activation barrier. Note that Na^+ ion in DEC:EC has an oxygen coordination ~ 3 and therefore based on the above argument is expected to have a higher activation barrier as shown in Figure 7.

In parallel with theoretical calculations, we conducted rate capability study on amorphous TiO_2/NT electrodes in Na half-cells with a variety of electrolytes. Figure 8 displays the Modified Peukert plot of TiO_2/NT electrodes cycled in 1 M NaClO_4 solutions of solvents (PC, EC:PC, EC:EMC, EC:DMC, and EC:DEC). We observed that the rate capability of TiO_2/NT electrodes in various electrolyte systems follow the order: EC:EMC > EC:DMC > EC:PC > PC > EC:DEC. As rate capability is dictated by how fast and efficient charge can be transported, our experimental results indicate that the EC:EMC and EC:DMC should have the lowest diffusion barrier and highest ionic conductivity among the studied electrolytes, which agrees well with our MD simulations. The dramatically low rate capability in EC:DEC compared to other systems might be related to the low transport number of Na^+ in EC:DEC. The rate capability studies thus confirm the importance of “kinetic effects” of the electrolytes on cell performance.

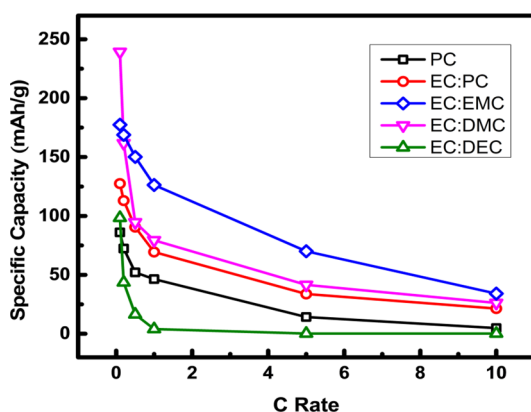


Figure 8. Modified Peukert plot for TiO_2/NT electrodes in various electrolyte systems.

e.) **Heat of Vaporization of Electrolytes.** Safety is an important consideration in the design of batteries and organic electrolytes generally have high volatility and flammability, which can pose serious safety issues. One of the important metrics of safety is the flammability of the vented electrolyte. It is a function of several variables such as temperature, pressure as well as solvent properties such as heat of vaporization, heat of combustion, and vapor pressure.⁴⁵ While the use of flame-retardant additive is an alternative, it has been shown to reduce the cell performance.⁴⁵ Mitigation of issues pertaining to flammability can be resolved by utilizing an inherently nonflammable or low-volatile electrolyte.

We extract the heat of vaporization for the various carbonates (pure components and their mixtures) and rank-order them to identify safe electrolytes. Figure 9(a) shows the calculated heat

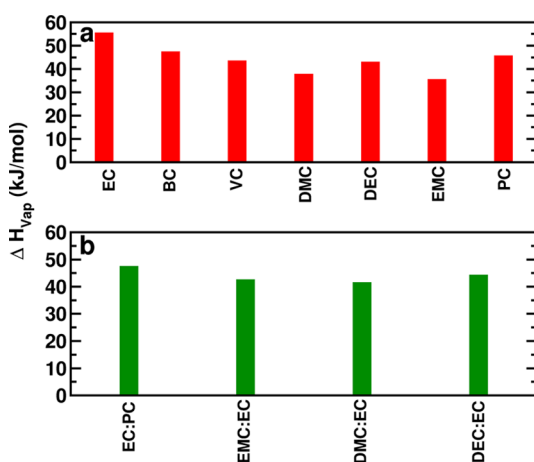


Figure 9. Estimated heats of vaporization for various pure and mixed solvents containing Na salts. In the case of mixed solvents, ΔH_{vap} is the amount of heat required to remove the more volatile component from the mixture. The standard deviation in the estimates is ~ 0.5 kJ/mol.

of vaporization for pure components. Electrolytes should have high heat of vaporization to be considered safe. EMC was found to be the worst electrolyte and its ΔH_{vap} is about 15 kJ/mol lower than EC, which performs the best among the simulated pure components. The heat of vaporization for pure component electrolytes follows the rank order (from more safe to least): $\text{EC} > \text{BC} > \text{PC} > \text{VC} \sim \text{DEC} > \text{DMC} > \text{EMC}$. Note that the quantitative estimates and the predicted rank order of the

simulations are in very good agreement with those reported experimentally (see Table 2).

Table 2. Computed heat of vaporization for the various pure component electrolytes in comparison to experimental values. The standard deviation is given in the parentheses

electrolyte	simulations (kJ/mol)	experiments (kJ/mol)
EC	55.12 (0.3)	51.68 ⁴⁶
PC	45.3 (0.6)	45.73 ⁴⁶
VC	43.2 (0.4)	41.4 ⁴⁶
DEC	42.73 (0.4)	41.96–44.76 ⁴⁷
DMC	37.50 (0.3)	36.53–38.56 ⁴⁷
EMC	35.22 (0.3)	34.63 ⁴⁶

We further estimate the heat of vaporization for the binary mixtures of EC:PC, EC:EMC, EC:DMC and EC:DEC. The same are plotted in Figure 9 (b) We find that the binary mixtures follow the rank order (from less to more volatile): $\text{EC:PC} > \text{EC:DEC} > \text{EC:EMC} > \text{EC:DMC}$. In general, we find that addition of the low-volatile pure component to EC to form a binary mixture resulted in the increase of ΔH_{vap} . Hence, the binary mixtures of PC, DEC, EMC, DMC with EC are expected to fare much better in the safety aspect when compared to their respective pure components. It should be noted that a more extensive rank-order scheme to include descriptors such as heat of combustion and heat release rate are required to comprehensively evaluate the electrolyte safety.⁴⁸ Efforts are underway to compute the same and will be reported in a separate study.

IV. CONCLUSIONS

We report an in silico-experimental pipeline strategy to determine the rank-order of different electrolyte formulations for Na^+ ion batteries. Several different cyclic and acyclic carbonate electrolytes (EC, PC, DMC, EMC, DEC), binary mixtures (EC:PC, EC:DMC, EC:EMC, and EC:DEC) and additives (VC, BC) with NaClO_4 as dissolved salt were benchmarked. Both thermodynamic and kinetic descriptors were used to establish some intrinsic trends and rationally arrive at optimal electrolyte formulations for Na^+ ion batteries. As a first rank-order criterion, PMF calculations were performed to calculate the free energy of solvation of the salt. Using free energy calculations as the thermodynamic descriptor to rank-order the various electrolyte combination, we arrive at EC:PC, EC:EMC and EC:DMC as the most suitable electrolytes. While thermodynamic descriptors help in identifying specific electrolyte formulations under equilibrium conditions, the use of kinetic descriptors as a transport metric is critical to identify electrolyte formulations with high power performance. Kinetic descriptors such as ionic conductivity and diffusion barrier based on the simulated MD trajectories were thus used to refine the rank-order of Na^+ ions in the various electrolytes. EC:DMC and EC:EMC emerged as the two most optimal electrolyte formulations among the various simulated carbonates.

A comprehensive atomistic picture of the solvation dynamics of Na^+ ions in the various electrolytes is derived from MD simulations and used to explain the atomistic origin of the observed trends in the thermodynamic and kinetic descriptors. At the atomistic level, the intricate relationship between the local coordination/solvation, the short-range ion–solvent interaction, and the long-range cation–anion interaction of

the Na salt dictate the observed energetics of ion solvation, the transport characteristics of the salt ions and degree of ion-pairing.

To verify our rank-order approach, cells were assembled with these various formulations (EC:PC, EC:DMC, EC:EMC, and EC:DEC) and state-of-the-art nanostructured TiO₂NT electrodes with NaClO₄ salt. Their electrochemical performance were evaluated and found to strongly correlate with the electrolyte formulation. Consistent with our computational predictions, EC:DMC and EC:EMC were found to be top electrolyte candidates for Na⁺ batteries and EC:DEC was found to be the worst. Our rate capability studies confirm that EC:DMC and EC:EMC to be the best formulations. These optimized formulations have specific capacities ~120–140 mAh/g whereas the lower ranked electrolytes (EC:DEC) have capacities ~95 mAh/g. While this could be attributed to the choice of the electrode, in future, our *in silico* approach will encompass explicit modeling and simulation of electrode with different electrolytes for an optimized Na ion electrode–electrolyte formulation. Our findings offer encouraging prospects for this approach in the *a priori* prediction of optimal Na⁺ ion systems with possible screening implications for novel electrolyte formulations for technologies that go beyond the standard Li⁺ ion while enabling in the mapping of electrode–electrolyte-genome database.

AUTHOR INFORMATION

Corresponding Authors

*E-mail: clairexiong@boisestate.edu.

*E-mail: skrssank@anl.gov.

Notes

The authors declare no competing financial interest.

ACKNOWLEDGMENTS

Use of the Center for Nanoscale Materials was supported by the U.S. Department of Energy, Office of Science, Office of Basic Energy Sciences, under Contract No. DE-AC02-06CH1135. This research used resources of the National Energy Research Scientific Computing Center, which is supported by the Office of Science of the U.S. Department of Energy under Contract No. DE-AC02-05CH11231.

REFERENCES

- (1) Thackeray, M. Lithium-Ion Batteries: An Unexpected Conductor. *Nat. Mater.* **2002**, *1*, 81–82.
- (2) Xu, K. Nonaqueous Liquid Electrolytes for Lithium-Based Rechargeable Batteries. *Chem. Rev.* **2004**, *104*, 4303–4417.
- (3) Tarascon, J. M.; Armand, M. Issues and Challenges Facing Rechargeable Lithium Batteries. *Nature* **2001**, *414*, 359–367.
- (4) Myounggu, P.; Xiangchun, Z.; Myoungdo, C.; Lessa, G. B.; Sastry, A. M. A Review of Conduction Phenomena in Li-Ion Batteries. *J. Power Sources* **2010**, *195*, 7904–7929.
- (5) Choi, N. S.; Chen, Z. H.; Freunberger, S. A.; Ji, X. L.; Sun, Y. K.; Amine, K.; Yushin, G.; Nazar, L. F.; Cho, J.; Bruce, P. G. Challenges Facing Lithium Batteries and Electrical Double-Layer Capacitors. *Angew. Chem., Int. Ed.* **2012**, *51*, 9994–10024.
- (6) Tarascon, J. M. Key Challenges in Future Li-Battery Research. *Philos. Trans. R. Soc., A* **2010**, *368*, 3227–3241.
- (7) Jeong, G.; Kim, Y. U.; Kim, H.; Kim, Y. J.; Sohn, H. J. Prospective Materials and Applications for Li Secondary Batteries. *Energy Environ. Sci.* **2011**, *4*, 1986–2002.
- (8) Armand, M.; Tarascon, J. M. Building Better Batteries. *Nature* **2008**, *451*, 652–657.
- (9) Wadia, C.; Albertus, P.; Srinivasan, V. Resource Constraints on the Battery Energy Storage Potential for Grid and Transportation Applications. *J. Power Sources* **2011**, *196*, 1593–1598.
- (10) Goodenough, J. B.; Kim, Y. Challenges for Rechargeable Batteries. *J. Power Sources* **2011**, *196*, 6688–6694.
- (11) Goodenough, J. B.; Kim, Y. Challenges for Rechargeable Li Batteries. *Chem. Mater.* **2010**, *22*, 587–603.
- (12) Whittingham, M. S. Lithium Batteries and Cathode Materials. *Chem. Rev.* **2004**, *104*, 4271–4301.
- (13) Levi, E.; Gofer, Y.; Aurbach, D. On the Way to Rechargeable Mg Batteries: The Challenge of New Cathode Materials. *Chem. Mater.* **2010**, *22*, 860–868.
- (14) Yoo, H. D.; Shterenberg, I.; Gofer, Y.; Gershinshy, G.; Pour, N.; Aurbach, D. Mg Rechargeable Batteries: An On-Going Challenge. *Energy Environ. Sci.* **2013**, *6*, 2265–2279.
- (15) Bruce, P. G.; Freunberger, S. A.; Hardwick, L. J.; Tarascon, J. M. Li-O-2 and Li-S Batteries with High Energy Storage. *Nat. Mater.* **2012**, *11*, 19–29.
- (16) Ji, X. L.; Nazar, L. F. Advances in Li-S Batteries. *J. Mater. Chem.* **2010**, *20*, 9821–9826.
- (17) Manthiram, A.; Fu, Y. Z.; Su, Y. S. Challenges and Prospects of Lithium-Sulfur Batteries. *Acc. Chem. Res.* **2013**, *46*, 1125–1134.
- (18) Slater, M. D.; Kim, D.; Lee, E.; Johnson, C. S. Sodium-Ion Batteries. *Adv. Funct. Mater.* **2013**, *23*, 947–958.
- (19) Yabuuchi, N.; Kajiyama, M.; Iwatate, J.; Nishikawa, H.; Hitomi, S.; Okuyama, R.; Usui, R.; Yamada, Y.; Komaba, S. P2-Type Na_x[Fe_{1/2}m_n1/2]O₂Made from Earth-Abundant Elements for Rechargeable Na Batteries. *Nat. Mater.* **2012**, *11*, 512–517.
- (20) Chevrie, V. L.; Ceder, G. Challenges for Na-Ion Negative Electrodes. *J. Electrochem. Soc.* **2011**, *158*, A1011–A1014.
- (21) Palomares, V.; Serras, P.; Villaluenga, I.; Hueso, K. B.; Carretero-González, J.; Rojo, T. Na-Ion Batteries, Recent Advances and Present Challenges to Become Low Cost Energy Storage Systems. *Energy Environ. Sci.* **2012**, *5*, 5884–5901.
- (22) Kim, S. W.; Seo, D. H.; Ma, X. H.; Ceder, G.; Kang, K. Electrode Materials for Rechargeable Sodium-Ion Batteries: Potential Alternatives to Current Lithium-Ion Batteries. *Adv. Energy Mater.* **2012**, *2*, 710–721.
- (23) Yildirim, H.; Greeley, J. P.; Sankaranarayanan, S. K. R. S. Concentration-Dependent Ordering of Lithiated Amorphous TiO₂. *J. Phys. Chem. C* **2013**, *117*, 3834–3845.
- (24) Yildirim, H.; Greeley, J. P.; Sankaranarayanan, S. K. R. S. The Effect of Concentration on Li Diffusivity and Conductivity in Rutile TiO₂. *Phys. Chem. Chem. Phys.* **2012**, *14*, 4565–4576.
- (25) Yildirim, H.; Greeley, J.; Sankaranarayanan, S. K. R. S. Effect of Concentration on the Energetics and Dynamics of Li Ion Transport in Anatase and Amorphous TiO₂. *J. Phys. Chem. C* **2011**, *115*, 15661–15673.
- (26) Ponrouch, A.; Marchante, E.; Courty, M.; Tarascon, J. M.; Palacin, M. R. In Search of an Optimized Electrolyte for Na-Ion Batteries. *Energy Environ. Sci.* **2012**, *5*, 8572–8583.
- (27) Ponrouch, A.; Dedryvere, R.; Monti, D.; Demet, A. E.; Mba, J. M. A.; Croguennec, L.; Masquelier, C.; Johansson, P.; Palacin, M. R. Towards High Energy Density Sodium Ion Batteries through Electrolyte Optimization. *Energy Environ. Sci.* **2013**, *6*, 2361–2369.
- (28) Komaba, S.; Murata, W.; Ishikawa, T.; Yabuuchi, N.; Ozeki, T.; Nakayama, T.; Ogata, A.; Gotoh, K.; Fujiwara, K. Electrochemical Na Insertion and Solid Electrolyte Interphase for Hard-Carbon Electrodes and Application to Na-Ion Batteries. *Adv. Funct. Mater.* **2011**, *21*, 3859–3867.
- (29) Aurbach, D.; Talyosef, Y.; Markovsky, B.; Markevich, E.; Zinigrad, E.; Asraf, L.; Gnanaraj, J. S.; Kim, H. J. Design of Electrolyte Solutions for Li and Li-Ion Batteries: A Review. *Electrochim. Acta* **2004**, *50*, 247–254.
- (30) Xiong, H.; Slater, M. D.; Balasubramanian, M.; Johnson, C. S.; Rajh, T. Amorphous TiO₂ Nanotube Anode for Rechargeable Sodium Ion Batteries. *J. Phys. Chem. Lett.* **2011**, *2*, 2560–2565.
- (31) Kamat, P. V. TiO₂ Nanostructures: Recent Physical Chemistry Advances. *J. Phys. Chem. C* **2012**, *116*, 11849–11851.

- (32) Yang, Z. G.; Choi, D.; Kerisit, S.; Rosso, K. M.; Wang, D. H.; Zhang, J.; Graff, G.; Liu, J. Nanostructures and Lithium Electrochemical Reactivity of Lithium Titanites and Titanium Oxides: A Review. *J. Power Sources* **2009**, *192*, 588–598.
- (33) Darve, E.; Pohorille, A. Calculating Free Energies Using Average Force. *J. Chem. Phys.* **2001**, *115*, 9169–9183.
- (34) Bhatnagar, N.; Kamath, G.; Chelst, I.; Potoff, J. J. Direct Calculation of 1-Octanol-Water Partition Coefficients from Adaptive Biasing Force Molecular Dynamics Simulations. *J. Chem. Phys.* **2012**, *137*, 014502.
- (35) Kamath, G.; Baker, G. A. In Silico Free Energy Predictions for Ionic Liquid-Assisted Exfoliation of a Graphene Bilayer into Individual Graphene Nanosheets. *Phys. Chem. Chem. Phys.* **2012**, *14*, 7929–7933.
- (36) Vanommeslaeghe, K.; et al. Charmm General Force Field: A Force Field for Drug-Like Molecules Compatible with the Charmm All-Atom Additive Biological Force Fields. *J. Comput. Chem.* **2010**, *31*, 671–690.
- (37) Henin, J.; Fiorin, G.; Chipot, C.; Klein, M. L. Exploring Multidimensional Free Energy Landscapes Using Time-Dependent Biases on Collective Variables. *J. Chem. Theory Comput.* **2010**, *6*, 35–47.
- (38) Phillips, J. C.; Braun, R.; Wang, W.; Gumbart, J.; Tajkhorshid, E.; Villa, E.; Chipot, C.; Skeel, R. D.; Kale, L.; Schulten, K. Scalable Molecular Dynamics with Namd. *J. Comput. Chem.* **2005**, *26*, 1781–1802.
- (39) Sankaranarayanan, S. K. R. S.; Ramanathan, S. Interface Proximity Effects on Ionic Conductivity in Nanoscale Oxide-Ion Conducting Yttria Stabilized Zirconia: An Atomistic Simulation Study. *J. Chem. Phys.* **2011**, *134*, 064703.
- (40) Xiong, H.; et al. Self-Improving Anode for Lithium-Ion Batteries Based on Amorphous to Cubic Phase Transition in TiO₂ Nanotubes. *J. Phys. Chem. C* **2012**, *116*, 3181–3187.
- (41) Xiong, H.; et al. Compositional Tuning of Structural Stability of Lithiated Cubic Titania Via a Vacancy-Filling Mechanism under High Pressure. *Phys. Rev. Lett.* **2013**, *110*, 078304.
- (42) Bockris, J. O. M.; Reddy, A. K. N. *Modern Electrochemistry*, 2nd ed.; Plenum Press: New York, 1998; Vol. 1.
- (43) *Linden's Handbook of Batteries*, 4th ed.; McGraw-Hill: New York, 2011.
- (44) Tarascon, J. M.; Guyomard, D. New Electrolyte Compositions Stable over the 0-V to 5-V Voltage Range and Compatible with the Li_{1+x}Mn₂O₄ Carbon Li-Ion Cells. *Solid State Ionics* **1994**, *69*, 293–305.
- (45) Roth, E. P.; Orendorff, C. How Electrolytes Influence Battery Safety. *Electrochem. Soc. Interface* **2012**, *Summer*, 45–49.
- (46) NIST. <http://webbook.nist.gov/chemistry/> (accessed May 7, 2014).
- (47) Kozlova, S. A.; Emel'yanenko, V. N.; Georgieva, M.; Verevkin, S. P.; Chernyak, Y.; Schäffner, B.; Börner, A. Vapour Pressure and Enthalpy of Vaporization of Aliphatic Dialkyl Carbonates. *J. Chem. Thermodyn. Thermochem.* **2008**, *40*, 1136–1140.
- (48) Eshetu, G. G.; Grugeon, S.; Laruelle, S.; Boyanov, S.; Lecocq, A.; Bertrand, J.-P.; Marlair, G. In-Depth Safety-Focused Analysis of Solvents Used in Electrolytes for Large Scale Lithium Ion Batteries. *Phys. Chem. Chem. Phys.* **2013**, *15*, 9145.